Ultra-fast switching blue phase liquid crystals diffraction grating stabilized by chiral monomer

Ramesh Manda[1]📧, **Srinivas Pagidi**[1], **Surjya Sarathi Bhattacharya**[2], **Hyesun Yoo**[1], **Arun Kumar T**[1], **Young Jin Lim**[1] **and Seung Hee Lee**[1,3]

[1] Applied Materials Institute for BIN Convergence, Department of BIN Convergence Technology and Department of Polymer Nano Science and Technology, Chonbuk National University, Jeonju, Jeonbuk, 561-756, Republic of Korea
[2] Asutosh College, 92, Shyamaprasad Mukherjee Road, Kolkata 700 026, West Bengal, India

E-mail: lsh1@chonbuk.ac.kr

Abstract

We have demonstrated an ultra-fast switching and efficient polymer stabilized blue phase liquid crystal (PS-BPLC) diffraction grating utilizing a chiral monomer. We have obtained a 0.5 ms response time by a novel polymer stabilization method which is three times faster than conventional PS-BPLC. In addition, the diffraction efficiency was improved 2% with a much wider phase range and the driving voltage to switch the device is reduced. The polarization properties of the diffracted beam are unaffected by this novel polymer stabilization. This device can be useful for future photonic applications.

Keywords: blue phase liquid crystals, polymer stabilization, chiral monomer, diffraction grating

[S] Supplementary material for this article is available online

(Some figures may appear in colour only in the online journal)

1. Introduction

Blue phase liquid crystals (BPLCs) have been extensively studied in display and photonic research due to their wide spread applications, such as spatial light modulators [1], optical inter-connectors in fiber optical communications [2, 3] beam splitters and steering applications [4, 5], and phase grating [6]. The great advantage of using BPLCs in optical devices is a fast response typically in sub-millisecond range, and naturally occurring optically isotropic field-off state [7]. Moreover, BPLC does not require an alignment layer and the material is cell gap insensitive, additionally a very large Kerr constant makes them the best candidates for future photonic applications. The efficiency of the diffraction device was drastically improved by utilizing the BPLC.

A typical BPLC system consists of self-assembly of double twist cylinders (DTC) forming a cubic structure with a lattice constant typically smaller than the visible wavelength, i.e. less than 300 nm. The three-dimensionally self-assembled DTCs cannot fill the whole cubic space; hence, formation of disclination lines in between cylinders is vital. The energetically highly stable disclinations lines limit the BP phase range to ~1 or 2 °C, which is too short for any practical applications. Hence, BPLCs are stabilized by a polymer network formation called polymer stabilized BPLCs (PS-BPLCs). The dispersed monomer molecule selectively inhibits the disclination lines by elastic interactions and sustains the cubic structure over a wide temperature range [8].

Interesting electro-optic properties have also been observed in another optically isotropic device like nano-structured polymer dispersed liquid crystals (nano-PDLC) in which the driving mechanism is governed by the strong anchoring of LC molecules at boundary surface [9, 10]. But the driving voltage

---

[3] Author to whom any correspondence should be addressed.

J. Phys. D: Appl. Phys. **51** (2018) 185103

R Manda *et al*

is higher and less concentration of LC involved leads to a smaller Kerr constant, which is a key parameter to control the driving voltage [11, 12]. The optimization of the phase separation method is also another crucial process which is notoriously difficult to control for obtaining a desired droplet size of LC [13, 14]. Compared with nano-PDLC, and among all other optically isotropic materials, the PS-BPLC is the best choice for making photonic devices.

The sharp rectangular phase profile resulting from the short coherence length of PS-BPLC appears to be advantageous for the fabrication of fast switching phase grating. A short coherence length of BPLC/PS-BPLC enables efficient reorientation of LC director subjected to field addressing in comparison with conventional nematic LC. Therefore, a larger refractive index modulation between successive electrodes induces a higher phase shift to the transmitted light resulting in efficient diffracting device. In addition, the response time is improved ~10 times in comparison with conventional diffractive device. By utilizing the advantages of BPLCs, several polarization independent [6, 16], 2D [15], large angle [17, 18], and transparent [19] diffraction gratings have been reported. However, the high driving voltage remains a critical issue for PS-BPLCs. The driving voltage could be decreased by employing high Kerr constant materials [20, 21], and novel electrode structures [22, 23], but it leads to a slow response and complexity of device fabrication, respectively. On the other hand, the response time of the device also needs to be improved further for future photonic applications.

Recently, we have reported a novel approach of BPLC stabilization using a chiral monomer [24]. It has been evidenced that chiral monomers reside in the double twist cylinder instead of disclination lines alone without disturbing the cubic lattice structure, as shown in figure 1. In the present report, we have used a similar polymer stabilization method and explored the effect of such a novel stabilized network over diffractive performance of the PS-BPLC device.

2. Theory

The periodic refractive index modulation of LC is the key parameter in optical phase gratings. In general, the refractive index modulation of LC is induced by a patterned electrode generated periodic electric field. The incident beam while traveling through such a spatially modulated director profile of LC under investigation undergoes spatially variable phase retardation, as well as rotation of plane of polarization. For optically isotropic materials, such as BPLC/PS-BPLC, the modulation of refractive index in response to the external field can be explained by the adopted Kerr effect [25]. A typical BPLC switching mechanism has been schematically shown in figures 2(a) and (b). At the field-off state, the BPLC exhibits optically isotropic phase, so the incident light experiences an isotropic refractive index (n_i). On field application, when positive LC is used, the LC molecules reorient and induce birefringence along the field direction. Here, the incident light experiences $n_e(E)$ refractive index along the field direction, and $n_o(E)$ refractive index orthogonal to field.

The variation of these three refractive indices in patterned electrodes switching has been shown in figures 2(a) and (b), and expressed as [26],

$$n_o(E) = n_i - \frac{\Delta n_{ind}(E)}{3}, n_e(E) = n_i + \frac{2\Delta n_{ind}(E)}{3}, \quad (1)$$

where $\Delta n_{ind}(E)$ is an induced birefringence at field E. The BPLC exhibits a sub-millisecond response time. Generally, the decay response time of the BPLC described by the following equation [27],

$$\tau_d \approx \frac{\gamma_1 P^2}{k_{eff}(2\pi)^2} \quad (2)$$

where γ_1 is the rotational viscosity of the host NLC, P is the chiral pitch, and k_{eff} is the effective elastic constant of NLC. The operating voltage of the BPLC system is inversely proportional to the square root of the Kerr constant. The Kerr constant can be expressed as [28],

$$K \approx \Delta n \Delta \varepsilon \frac{\varepsilon_o P^2}{k_{eff} \lambda (2\pi)^2} \quad (3)$$

where $\Delta \varepsilon$ is the dielectric anisotropy, ε_o is the dielectric permittivity of free space, and λ is the wavelength of incident light. The Kerr constant directly proportional to the Δn, $\Delta \varepsilon$, and P^2. Therefore, the high birefringence and high dielectric anisotropic LC provides a high Kerr constant, which is an essential parameter to reduce the driving field. The smaller chiral pitch LC provides a low Kerr constant. In a conventional polymer stabilization method, monomers selectively occupy the disclinations lines and polymerize them, resulting in the formation of polymer networks only in disclinations. On the contrary, in our approach, the chiral monomer is occupied not only in disclinations but also inside the DTCs. In this case, polymerization of chiral monomer would form a random network inside the DTC and disclinations together without breaking the cubic symmetry of BP. Here, the polymer network interacts more closely with the LC molecules so that it strongly influences the electro-optical properties.

The selective Bragg reflection is of the characteristic nature of the BPLC. When light passes through the BPLC medium, a narrow band Bragg reflection occurs from self-assembled periodic Bravais lattices. For an angle of incidence normal to the substrate, the Bragg reflection can be expressed as [29],

$$\lambda = \frac{2\bar{n}a}{\sqrt{x^2 + y^2 + z^2}} \quad (4)$$

where λ is the Bragg reflection wavelength, $\bar{n}$ is the average refractive index of the NLC, and a is the lattice constant ($a = P$ for BPI, and $a = P/2$ for BPII). The x, y, and z are miller indices of the Bravais lattice which are orthogonal to each other.

The diffraction efficiency was defined as the ratio between the incident light and particular diffraction orders, expressed as,

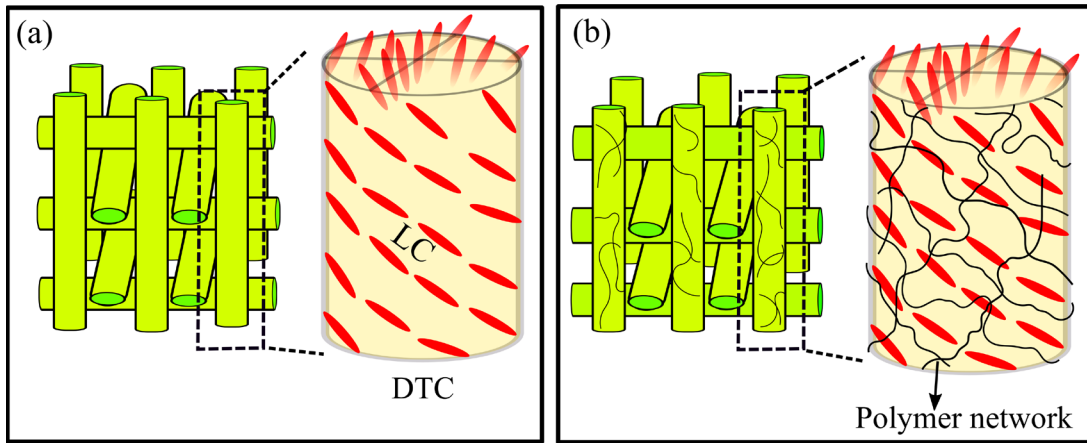$$\eta(\%) = \frac{I_m}{I_{total}} \times 100 \quad (5)$$

J. Phys. D: Appl. Phys. **51** (2018) 185103

R Manda *et al*

Figure 1. Schematic representation of BPLC stabilization. (a) Conventional model and (b) proposed model.
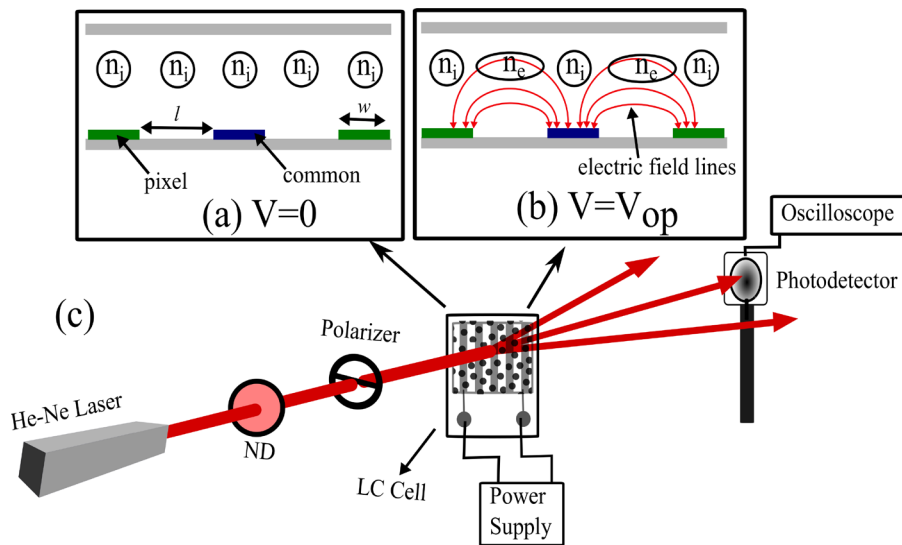

Figure 2. Typical switching mechanism of the BPLC with in-plane switching (IPS) cell, (a) at zero field, (b) at driving field, and (c) schematic representation of the experimental setup to measure diffraction efficiency. The photodetector is replaced by a screen to capture the diffraction images. ND is neutral density filter.

Table 1. Material concentrations used in this report.

	BPLC				
Sample	MLC2053 (wt%)	SRM17[a](wt%)	TMPTA[b] (wt%)	SRM03[c] (wt%)	Irgacure907[d] (wt%)
PS-BP1	88	4	7	—	1
PS-BP2	88	4	—	7	1

[a] SRM17 is a chiral dopant with HTP $\approx 166 \ \mu m^{-1}$.
[b] TMPTA is a photo reactive monomer having no chiral property.
[c] SRM03 is a photo reactive chiral monomer with HTP $\approx 11 \ \mu m^{-1}$.
[d] Irgacure907 is a photo-initiator.

where I_m is intensity of mth order ($m = 1, 2, 3, 4, ..$), and I_{total} is the intensity of incident light. The diffraction angle can also be measured by using the well known grating equation, $\sin\theta = \frac{m\lambda}{n(E)\Lambda}$, where Λ is a pitch of the refractive index.

3. Experiments

The BPLC mixture has been prepared by mixing a high dielectric anisotropy nematic liquid crystal mixture, viz.

MLC2053 ($\Delta\varepsilon = 42.6$, $\Delta n = 0.235$, and $T_{NI} = 86$ ∘C, from Merck Advanced Technology in Korea) and chiral dopant, SRM17 (helical twist power (HTP) $\sim 166 \ \mu m^{-1}$). We have used monomer TMPTA (Trimethylolpropane Triacrylate, Sigma-Aldrich), and chiral monomer SRM03 ((HTP) $\sim 11 \ \mu m^{-1}$) to stabilize the BP phase. The SRM17 is the chiral dopant while the SRM03 plays both roles as photo-polymer and chiral dopant. A small amount of photo-initiator, Irgacure907, was utilized to initiate the polymerization process. The details
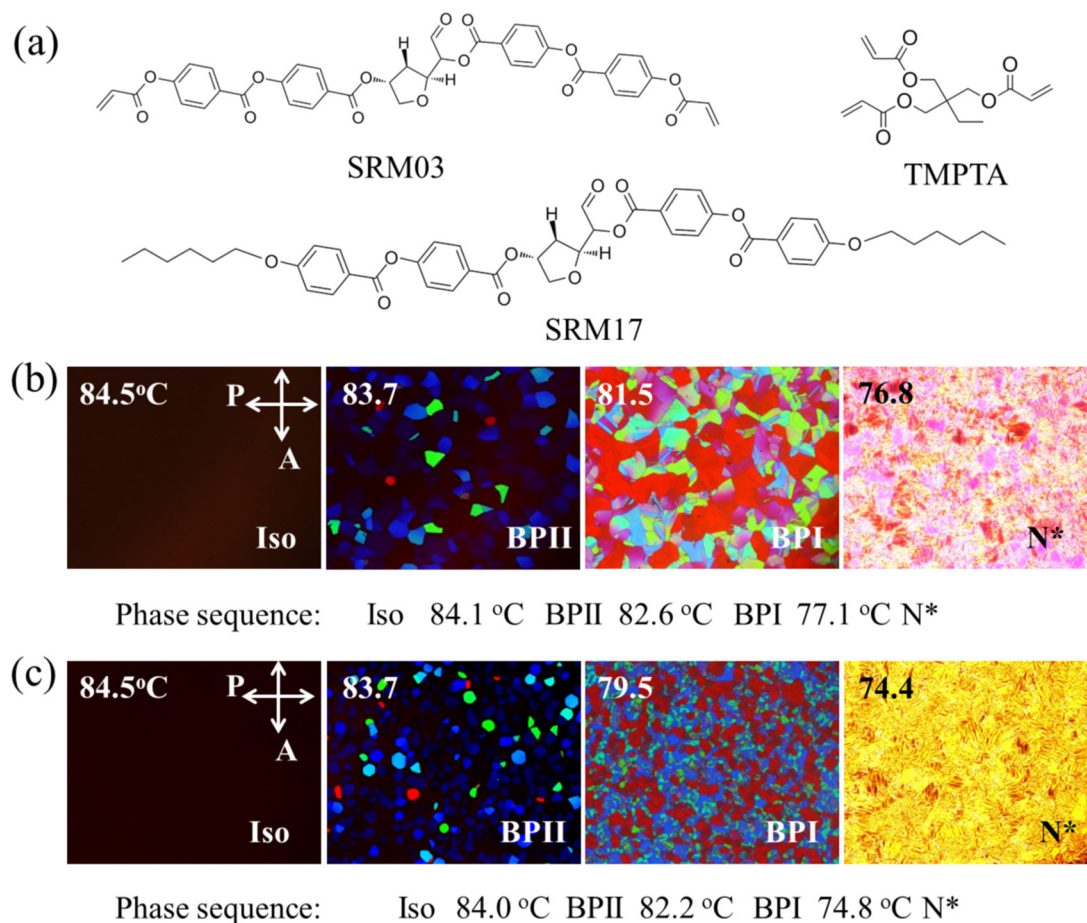
J. Phys. D: Appl. Phys. **51** (2018) 185103

R Manda *et al*

Figure 3. (a) Molecular structure of chiral dopant (SRM17), monomer (TMPTA), and chiral monomer (SRM03). Phase sequence and POM images of (b) PS-BP1 and (c) PS-BP2 as functions of temperature cooling from isotropic phase.

regarding the concentration of the monomer, chiral monomer and photo-initiator are summarized in table 1. The molecular structures of the material used in this report have been shown in figure 3(a).

An in-plane switching (IPS) cell was used for optical microscopic and electro-optic characterization of the PS-BPLC sample. The obtained homogeneous mixture was injected into the IPS cell at an isotropic temperature, viz. 90 °C, by capillary action. The polymerization process of monomer mixed BP sample is accomplished in 5 min under 50 mW/cm^{-2} intense UV light of 365 nm wavelength, while the BPII phase of the sample was kept unaltered by temperature control. We have used a highly efficient temperature controller (INSTEC, HSC402-STC20U) to control the polymerization to realize polymer stabilization and further electro-optic characterization of the BP phase. The IPS cell used for the present experiments consists of 4 μm wide interpenetrating comb shaped bottom electrodes maintaining a separation of 4 μm between electrodes while the top substrate does not have any electrodes. Uniform separation between the two substrates was fixed to 10 μm using a silicon ball spacer.

BPLC filled IPS test cells were placed between crossed polarizers of a polarizing optical microscope (POM) (Nikon, ECLIPSE E600) attached with a CCD camera (Nikon, DXM 1200). Hence, optical micrographs of the sample were captured while decreasing the temperature with the cooling rate

0.3 °C min^{-1}. The experimental set-up for measurement of the electric field induced transmission consists of a He–Ne laser ($\lambda = 632.8$ nm) source followed by the polarizer, BPLC filled IPS test-cell, and photodetector connected with a digital storage oscilloscope (Tektronix, DPO2024B) as depicted in figure 2(c). The incident light polarization is perpendicular to the long IPS electrode, i.e. TM mode. Test cells are subjected to a square wave signal generated using a function generator (Tektronix, AFG3101C) and modulated by an amplifier (FLC Electronics, A400). The change in transmission through the test cells in response to the applied 1 kHz square wave field is recorded by photo diodes and stored in the digital storage oscilloscope. A screen is placed 72 cm behind the test cells to realize the far field diffraction and imaging purposes. The diffraction pattern projected on the screen was recorded with a high resolution camera (Samsung, NX1000). The polarization state was characterized by placing the analyzer behind cell. At the field-on state, the analyzer is rotated in a counterclockwise direction and transmittance was measured with the photo-diode and oscilloscope. The response time was measured by observing transmittance change due to electric field, on and off. Finally, we have characterized the polymer network structure by using a field emission scanning electron microscope (FESEM). The sample cells were kept immersed in hexane for 48 h to wash-out LC molecules and the two substrates were separated. A carbon layer was coated on the film
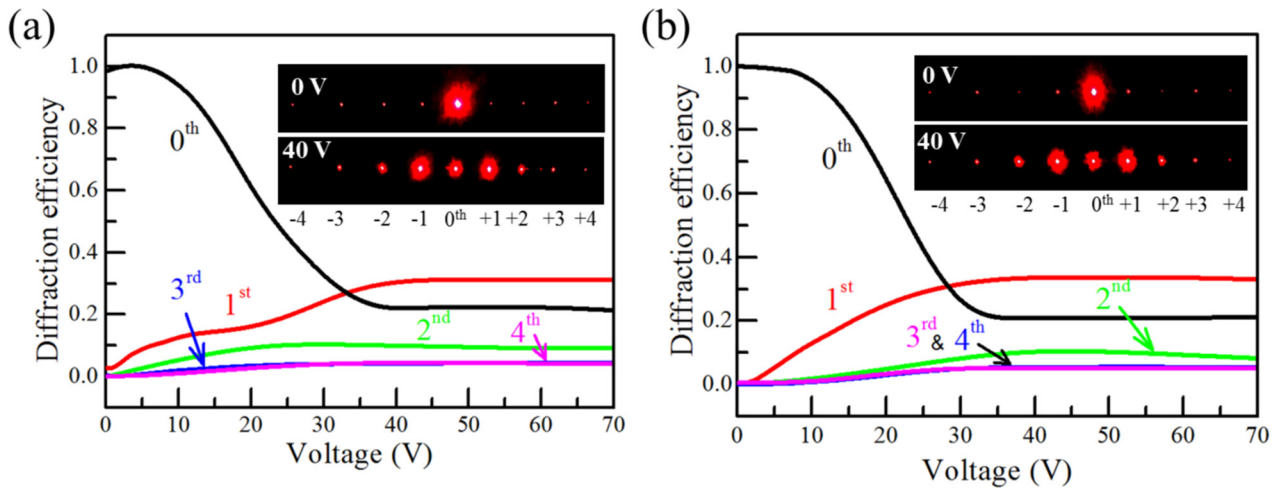
J. Phys. D: Appl. Phys. **51** (2018) 185103

R Manda *et al*

Figure 4. Diffraction efficiencies and corresponding diffraction patterns (inserted) of (a) PS-BP1, and (b) PS-BP2. The temperature was set to 79.5 °C. Diffraction efficiency defined as equation (5).

to make electric contact with the polymer network and images observed normal to the substrate.

4. Results and discussion

The characteristic platelet structure was observed in both samples under POM, as shown in figure 3(b). The observed phase sequence has been confirmed by temperature controlled POM imaging. The PS-BP1 exhibits a 5.5 °C wide BPI and a 1.5 °C wide BPII phase, while the PS-BP2 shows a 7.4 °C wide BPI and a 1.8 °C wide BPII. The cumulative range or polymer stabilized BP phases for sample 1 and 2 are 7 °C and 9.2 °C, respectively. By comparing both sequences, one can notice that the BPI phase was found to appear in a wider range than BPII in both the samples. BPII consists of mostly blue colored platelets in both samples. In BPI, a major portion of the sample was found to be covered by red color platelets in PS-BP1, and by an equal quantity of blue and red color platelets in PS-BP2. By comparing both PS-BP1 and PS-BP2, one can clearly notice that the reflection wavelength of the BPII is not much affected by chiral monomer. On the contrary, the reflection wavelength of BPI is shifted to a shorter wavelength (yellowish to blue color). From equation (4), for PS-BP2, it implies that the lattice constant *a* is slightly altered. Finally, from POM images, we conclude that the 3D structure of BPLC lattice is slightly affected by the chiral monomer.

Polarized He–Ne laser beam made incident on test-cells in plane perpendicular to the patterned electrode of the IPS substrate and the intensity of the light transmitted through the cell in such a configuration were detected by the photodetector and recorded in the digital storage oscilloscope as depicted in figure 2(c). A screen was placed behind the cell to capture the diffracted images. The distance between the cell to screen is nearly 72 cm. The diffraction efficiency was measured by using the photodetector. The temperature for both samples was fixed at 79.5 °C, ensuring BPI phase. All diffraction properties have been characterized in the BPI phase.

Inset of figures 4(a) and (b) shows photographic images of diffraction patterns for the PS-BP1 and PS-BP2 samples

in driving voltage off and the same under 40 V drive, respectively. Evidently, in the field-off state, a major portion of incident beam transmitted through the cell and concentrated on the 0th order with weak diffraction spots appears on either side of 0th order, due to the refractive index mismatch of electrode patterns and glass substrate. At the field-on state, the periodic modulation of the refractive index makes a periodic phase shift of the transmitted light that resulted in transfer of 0th order intensity to higher orders. The higher orders symmetrically appear on both sides of the 0th order in both samples. The spatial frequency of the diffracted beam determined by the pitch (Λ) of the IPS cell, which is equal to sum of electrode width (*w*) and spacing (*l*).

The diffraction efficiency has been measured following equation (5) and found to be 31% and 33% for positive 1st order beams of PS-BP1 and PS-BP2, respectively, in the BPI phase. A small reduction in the driving voltage was noticed in PS-BP2. A possible reason for the decrease in driving voltage in PS-BP2 is due to the slightly enhanced Kerr constant. Enhanced diffraction efficiency by ~2% for PS-BP2 may be due to a more precisely followed director profile to the field enforcing higher refractive index difference between the electrode and non-electrode regions.

We have determined the polarization state of each diffraction order in both the PS-BP1 and PS-BP2 samples. The polarization state of samples PS-BP1 and PS-BP2 are shown in figures 5 and 6, respectively. The incident light is linearly polarized and the polarization direction is perpendicular to the long side IPS electrodes i.e. TM mode. Hence, the incident beam vibrates in the *x-z* plane while propagating along the *z*-axis in a right handed rectangular Cartesian coordinate system. The analyzer was fixed behind the cell and the polarization properties are confirmed by rotating the analyzer in a counter-clockwise sense in the *x-y* plane. The measured analyzer's angle was referred with respect to the *y*-axis. The intensity change of the diffracted light was detected by the photodiode and digital storage oscilloscope.

Usually, the zero intensity corresponding to crossed polarizers, i.e. the analyzer's angle is 90° with respect to polarizer,
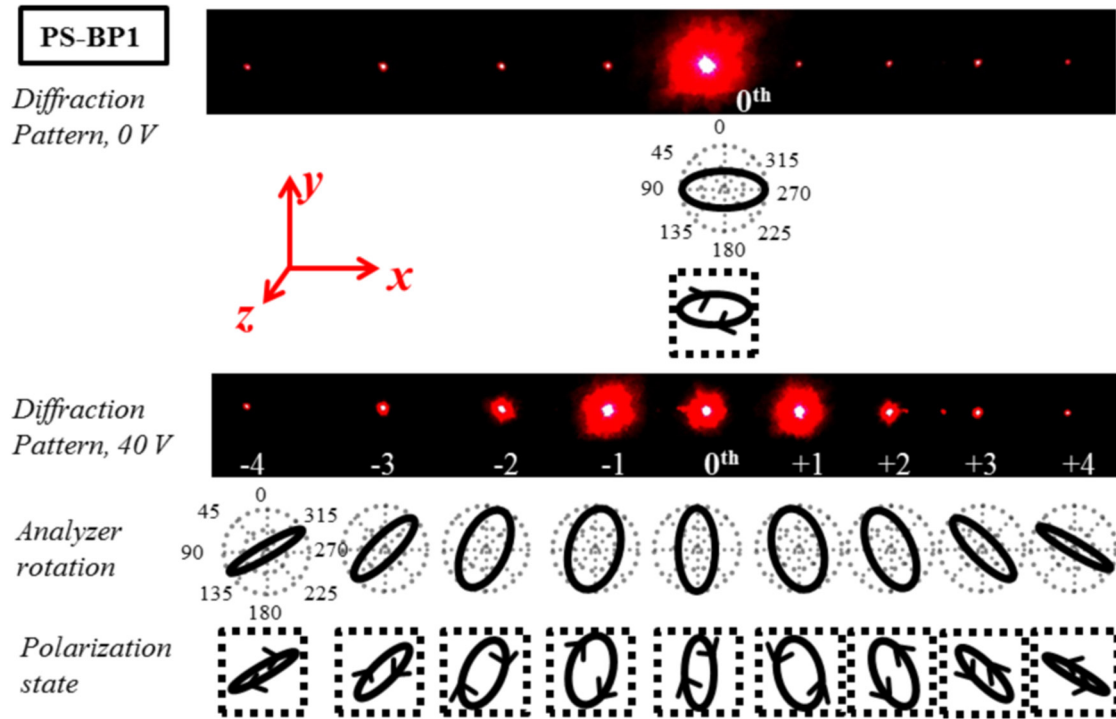
J. Phys. D: Appl. Phys. **51** (2018) 185103

R Manda *et al*

Figure 5. The polarization states of the PS-BP1 sample at 0 V and 40 V. The temperature was set to 79.5 °C, i.e. BPI phase is investigated.
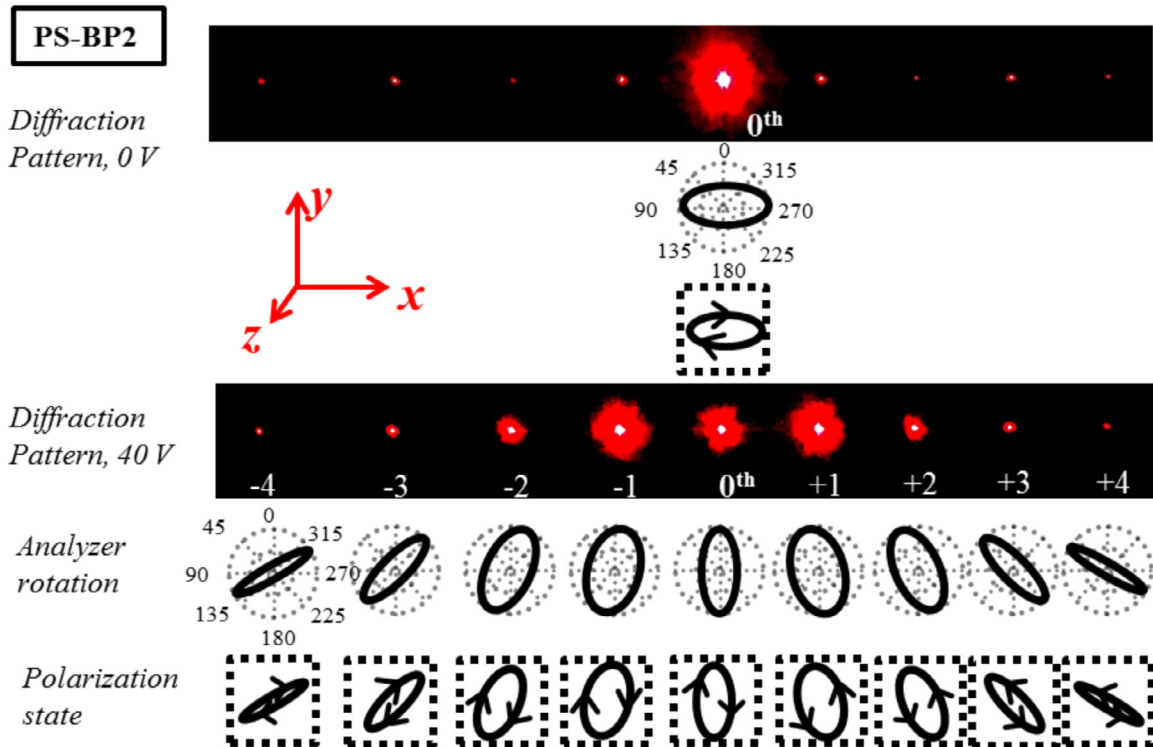

Figure 6. The polarization states of the PS-BP2 sample at 0 V and 40 V. The temperature was set to 79.5 °C, i.e. the BPI phase is investigated.

is assumed to be linear polarization. The intensity unaffected by the analyzer's angle is assumed to be a circular polarization. The elliptical polarization state is characterized by two parameters; ellipticity of the respective diffracted orders and the inclination of ellipses with respect to the polarization plane of incident beam viz. called ellipse/azimuthal angle.

The ellipticity is zero for linear polarization and 1 for circular polarization. Here, the ellipticity is estimated from the ratio of intensity of diffracted light along the *x-z* and *y-z* planes when the analyzer is rotated in a counter-clockwise direction. The ellipse angle is estimated from the analyzer's angle corresponding to the maximum intensity with respect to the *y*-axis.

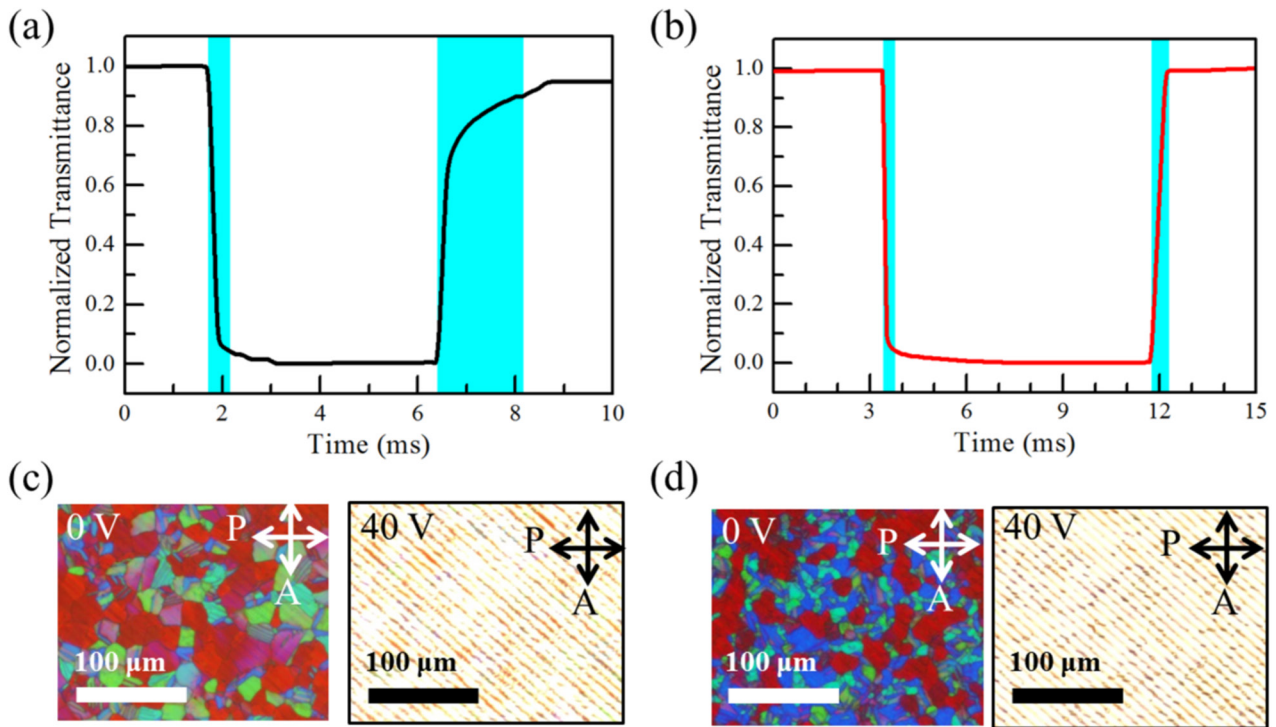J. Phys. D: Appl. Phys. **51** (2018) 185103

R Manda *et al*

Figure 7. The first order response time of (a) PS-BP1 and (b) PS-BP2. The switching images of (c) PS-BP1 and (d) PS-BP2 under crossed polarizers. The long ITO electrode strip was set to 45° to polarizer to see the platelet structure. The temperature was fixed to 79.5 °C for both samples.

Another important parameter, the handedness or direction of the polarization state is confirmed by observing variations in diffracted light intensity with the applied field when the analyzer's angle set at −45° with respect to the *y*-axis for both the positive and negatives orders.

We have investigated the polarization properties of BPI phase with driving field and without field. We have also observed the beam properties when the sample is above T_{NI}. In PS-BP1, the polarization state of the diffracted beam is found to be linear and the polarization angle coincides with the incident light when the sample is in isotropic phase (above T_{NI}). In other words, the polarization state of the incident beam is unaffected by the sample at above T_{NI} of NLC. On the contrary, although BPLC is optically isotropic, the polarization state of the diffracted beam changed to elliptical polarization when the sample cooled down to BP, but the ellipse angle of polarized beam is found to coincide with the incident beam, as shown in figure 5, and also shown in supplementary material figure S1(a) (stacks.iop.org/JPhysD/51/185103/mmedia). A similar trend observed for the sample PS-BP2 as well, as shown in figure 6, is also shown supplementary materials figure S1(b). This could be due to the optical rotary power that was induced from the local anisotropic nature of BPLC. Hence, the evident polarization state is modified by the platelet structure. The polarization state of 0th order remains unchanged on field application but the ellipse angle is found to be rotated by 90° in both the samples as evident in figure 5 (shown in figure S1(a)) and a similar trend was observed for PS-BP2 figure 6 (shown in figure S1(b)).

Similarly, we also measured the polarization properties of higher diffraction orders of both the PS-BP1 and PS-BP2

samples. The higher orders are also elliptically polarized but the ellipticity and ellipse angle are different from one another as shown in figure 5 (shown in figures S2(a) and(c)). The PS-BP2 samples also shows a similar behavior, as shown in figure 6 (and shown in figures S2(b) and (d)). The handedness of the polarization state was confirmed by comparing the voltage dependent transmittance of the positive and corresponding negative order for the fixed analyzer's angle. Here, we fixed the analyzer angle at −45° with respect to the *y*-axis and measured both +1st and −1st orders, shown in supplementary material figure S3. The +1 and −1 orders show the different intensity profiles for the fixed analyzer's angle. We assume that this difference is only attributed from the variation in handedness of the polarization state. Similarly, we also measured handedness of the polarization for the remaining higher orders. By comparing all higher orders of the sample, one can easily realize that the polarization states of negative and positive orders are mirrored symmetric to each other. Overall, we conclude that the state of polarization of diffracted beam is not altered by the chiral monomer. Interestingly, like diffraction orders, the polarization properties of the diffracted beam such as ellipticity and ellipse angles are also spatially distributed in both cases. In other words, the ellipse angle is rotated ∼0° to ∼60° from 0th order to 4th order, respectively. Therefore, we can conclude that the ellipticity and ellipse angle of polarization could be spatially modulated by the external field.

We have measured the response time of 0th orders of both samples and the obtained results are shown in figures 7(a) and (b). The rise time and decay time are defined as the time taken for 10%–90% transmittance change while increasing the field
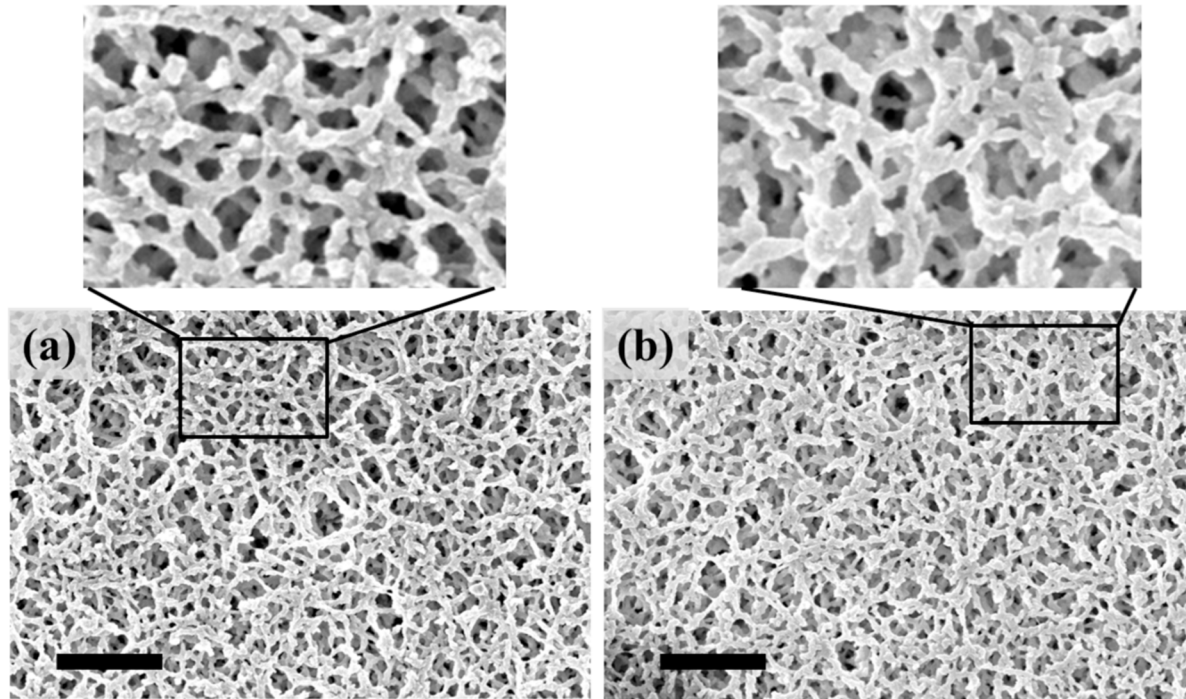
J. Phys. D: Appl. Phys. **51** (2018) 185103

R Manda *et al*

Figure 8. Observed microstructure of (a) PS-BP1 and (b) PS-BP2. The represented scale bar is equal to 1 μm.

and 90%–10% transmittance change while decreasing the field, respectively. The measured rise times are 0.19 ms and 0.13 ms for PS-BP1 and PS-BP2, respectively. The measured decay times are 1.73 ms and 0.37 ms for PS-BP1 and PS-BP2, respectively. The PS-BP2 sample decay response is 3 times faster than PS-BP1. The PS-BPLC stabilized by chiral monomer shows a fast response time and a high diffraction efficiency in comparison with conventional PS-BPLC.

The POM images of the PS-BP1 and PS-BP2 under crossed polarized conditions was shown in figures 7(c) and (d), respectively. The periodic bright and dark lines represent the director field with pitch length Λ. According to equation (2), the fast decay time for PS-BP2 might be due to change in chiral pitch (P) induced by an additional twist imposed by the chiral monomer. Moreover, the surface anchoring energy of the conventional polymer stabilized sample, PS-BP1, is smaller and can easily be neglected in comparison with elastic free energy. But, in our case, the polymer network occupied inside the DTC, so we strongly believe that the anchoring energy would definitely bring considerable change to the total free energy, due to the strong elastic tourque induced between the LC and polymer network. Therefore, it cannot be neglected as a conventional one. The fast decaying time is due to the strong anchoring energy between LC and polymer in PS-BP2. Another possible reason for fast response is the decrease in coherence length due to polymerization of chiral monomer inside the DTC.

Finally, we have observed the obtained polymer microstructure for both the PS-BP1 and PS-BP2 samples by using FESEM. The cells were immersed in hexane for 48 h, dried up and two substrates separated with sharp edged blade. The scanning electron microscopic results obtained from carbon coated films are depicted in figure 8. The results suggest that there is a slight change in density of polymer microstructure. The density of the polymer network is measured with ImageJ software, a java-based image processing program developed at the National Institutes of Health. The estimated area occupied by the polymer network was found to be increased from ~48% to ~53% for PS-BP1 to PS-BP2, respectively. We have also measured the size of the polymer network strand. The measured average size of the polymer network strand varies from 30 nm to 70 nm for PS-BP1, whereas 50 nm–110 nm for PS-BP2. The density of the polymer network of PS-BP2 seems to be higher than the PS-BP1. The increase in density of the network might have resulted from the polymerization of monomer molecules inside the DTC structure, instead of disclinations lines alone. Although, FESEM data are not direct proof for chiral monomer occupying inside the DTC structure, a noticeable enhancement in the network density might be indicative of the anticipated result.

5. Conclusion

We have demonstrated an ultra-fast switching of PS-BPLC diffraction grating stabilized utilizing chiral monomers at which the dispersed chiral monomer polymerizes while staying inside the DTC instead of disclinations alone. Even though we have employed high dielectric anisotropic liquid crystals, the measured response time of the proposed device is in the sub-millisecond range (~0.5 ms) and it is three times faster than conventional PS-BPLC. The diffraction efficiency was improved by 2% with a wider phase range and a considerable decrease in driving voltage was noticed. The polarization properties of the diffracted beam is studied in detail. These fast response diffraction gratings are highly desirable in future photonic devices.

J. Phys. D: Appl. Phys. **51** (2018) 185103

R Manda *et al*

Acknowledgments

ORCID iDs

Ramesh Manda https://orcid.org/0000-0002-6171-7991

References

[1] Peng F, Lee Y H, Luo Z and Wu S T 2015 *Opt. Lett.* **40** 5097
[2] Khoo I C, Hong K L, Zhao S, Ma D and Lin T H 2013 *Opt. Express* **21** 4319
[3] Lin C H, Wang Y Y and Hsieh C W 2011 *Opt. Lett.* **36** 502
[4] Ren H, Fan Y H and Wu S T 2003 *Appl. Phys. Lett.* **82** 3168
[5] Chen H, Weng Y, Xu D, Tabiryan N V and Wu S T 2016 *Opt. Express* **24** 7287
[6] Zhu G, Li J N, Lin X W, Wang H F, Hu W, Zheng Z G, Cui H Q, Shen D and Lu Y Q 2012 *J. Soc. Inf. Disp.* **20** 341
[7] Chen Y, Yan J, Sun J, Wu S T, Liang X, Liu S H, Hsieh P J, Cheng K L and Shiu J W 2011 *Appl. Phys. Lett.* **99** 201105
[8] Kikuchi H, Yokota M, Hisakado Y, Yang H and Kajiyama T 2002 *Nat. Mater.* **1** 64
[9] Choi S W, Yamamoto S I, Iwata T and Kikuchi H 2009 *J. Phys. D: Appl. Phys.* **42** 112002
[10] Tanabe Y, Furue H and Hatano J 2005 *Mater. Sci. Eng.* B **120** 41
[11] Yang Y C and Yang D K 2011 *Appl. Phys. Lett.* **98** 023502
[12] Rao L, Yan J and Wu S T 2010 *J. Soc. Inf. Disp.* **18** 954
[13] Ohta S, Inasawa S and Yamaguchi Y 2012 *J. Poly. Sci.* B **50** 863
[14] Manda R, Pagidi S, Kim M, Park C H, Yoo H S, Sandeep K, Lim Y J and Lee S H 2017 *Liq. Cryst.* **45** 736
[15] Zhu J L, Lu J G, Qiang J, Zhong E W, Ye Z C, He Z, Guo X, Dong C Y, Su Y and Shieh H P 2012 *J. Appl. Phys.* **111** 033101
[16] Yan J, Li Q and Hu K 2013 *J. Appl. Phys.* **114** 153104
[17] Yan J, Xing Y and Li Q 2015 *Opt. Lett.* **40** 4520
[18] Gao L, Zheng Z Z, Zhu J L, Han W M and Sun Y B 2016 *Opt. Lett.* **41** 3775
[19] Manda R, Pagidi S, Bhattacharyya S S, Park C H, Lim Y J, Gwag J S and Lee S H 2017 *Opt. Express* **25** 24033
[20] Rao L, Yan J, Wu S T, Yamamoto S I and Haseba Y 2011 *Appl. Phys. Lett.* **98** 081109
[21] Chen Y, Xu D, Wu S T, Yamamoto S I and Haseba Y 2013 *Appl. Phys. Lett.* **102** 141116
[22] Jiao M, Li Y and Wu S T 2010 *Appl. Phys. Lett.* **96** 011102
[23] Rao L, Ge Z, Wu S T and Lee S H 2009 *Appl. Phys. Lett.* **95** 231101
[24] Manda R, Kim M S, Shin E J, Gong M S, Murali G, Sandeep K, Lee M H, Lee J H and Lee S H 2017 *Liq. Cryst.* **44** 1059
[25] Yan J, Cheng H C, Gauza S, Li Y, Jiao M, Rao L and Wu S T 2010 *Appl. Phys. Lett.* **96** 071105
[26] Yan J, Jiao M, Rao L and Wu S T 2010 *Opt. Express* **18** 11450
[27] Gleeson H F and Coles H J 1989 *Liq. Cryst.* **5** 917
[28] Gerber P R 1985 *Mol. Cryst. Liq. Cryst.* **116** 197
[29] Kato T 2008 *Liquid Crystalline Functional Assemblies and Their Supramolecular Structures* (New York: Springer) pp 99–117